Bottom-up synthesis of carbon nanoparticles with higher doxorubicin efficacy

Samer Bayda [a,b], Mohamad Hadla [a,c], Stefano Palazzolo [a,b], Vinit Kumar [a,d], Isabella Caligiuri [a], Emmanuele Ambrosi [e,f], Enrico Pontoglio [e,f,g], Marco Agostini [h,i], Tiziano Tuccinardi [j], Alvise Benedetti [e,f], Pietro Riello [e,f], Vincenzo Canzonieri [a], Giuseppe Corona [a], Giuseppe Toffoli [a], Flavio Rizzolio [a,*]

[a] Department of Translational Research, National Cancer Institute - CRO-IRCCS, Aviano, Italy
[b] Doctoral School in Nanotechnology, University of Trieste, Italy
[c] Doctoral School in Pharmacological Sciences, University of Padova, Italy
[d] Amity Institute of Molecular Medicine & Stem Cell Research, Amity University, Noida, India
[e] Department of Molecular Sciences and Nanosystems and Electron Microscopy Center "Giovanni Stevanato", University Ca' Foscari of Venezia, Italy
[f] European Center of Living Technology, Venezia-Mestre, Italy
[g] Doctoral School in Chemistry, University of Trieste, Italy
[h] Department of Surgical, Oncological and Gastroenterological Sciences, Section of Surgery, University of Padova, Italy
[i] Pediatric Research Institute, Città della Speranza, Padova, Italy
[j] Department of Pharmacy, University of Pisa, Italy

ARTICLE INFO

Keywords:
Carbon nanoparticles
Cancer
Drug delivery
Nanotechnology
Doxorubicin

ABSTRACT

Nanomedicine requires intelligent and non-toxic nanomaterials for real clinical applications. Carbon materials possess interesting properties but with some limitations due to toxic effects. Interest in carbon nanoparticles (CNPs) is increasing because they are considered green materials with tunable optical properties, overcoming the problem of toxicity associated with quantum dots or nanocrystals, and can be utilized as smart drug delivery systems. Using black tea as a raw material, we synthesized CNPs with a narrow size distribution, tunable optical properties covering visible to deep red absorption, non-toxicity and easy synthesis for large-scale production. We utilized these CNPs to label subcellular structures such as exosomes. More importantly, these new CNPs can escape lysosomal sequestration and rapidly distribute themselves in the cytoplasm to release doxorubicin (doxo) with better efficacy than the free drug. The release of doxo from CNPs was optimal at low pH, similar to the tumour microenvironment. These CNPs were non-toxic in mice and reduced the tumour burden when loaded with doxo due to an improved pharmacokinetics profile. In summary, we created a new delivery system that is potentially useful for improving cancer treatments and opening a new window for tagging microvesicles utilized in liquid biopsies.

1. Introduction

Nanoparticle technology is an attractive field at the forefront of research and plays important roles in medicine, agriculture and electronics. Nanoparticles have wide applications in medicinal fields as nanocarriers for drug delivery and agents for multifunctional diagnosis, for example [1,2]. Recently, a new class of carbon nanomaterials, including nanodiamonds [3] and fluorescent carbon nanoparticles (CNPs) [4], have been widely investigated due to their high hydrophilicity, excellent biocompatibility, good cell permeability, high photostability and flexibility in surface modification as a result of the presence of different functional groups (carboxyl, hydroxyl and amino groups), allowing the covalent conjugation of chemotherapeutic and targeting agents [5]. Particularly, fluorescent CNPs have wide applications in areas such as bioimaging, drug delivery [6–10], sensors [11–14], optoelectronics [15] and photocatalysis [16]. CNPs are comparable to quantum dots (QDs) and organic dyes [17]. QDs are semiconductor nanostructures with unique optical and electrical properties and great flexibility in their bright and tunable photoluminescence. The blinking effect is a problem with QDs that can be overcome by surface passivation or core-shell formation [18]. QDs are composed of heavy metal precursors such as selenium (Se) and cadmium (Cd), which are toxic at low concentrations in the human body and environment [17,19]. The use of CNPs in place of QDs might overcome the above mentioned problems. Notably, CNPs have attracted considerable interest, as they offer

* Corresponding author at: Clinical Pharmacology, Department of Molecular Biology and Translational Research, National Cancer Institute and Center for Molecular Biomedicine, CRO Aviano (PN), Via Franco Gallini, 2, Aviano 33081, PN, Italy.
E-mail address: frizzolio@cro.it (F. Rizzolio).

potential advantages over the other carbon nanomaterials such as carbon nanotubes [20–22] and Halloysite nanotubes [23,24] including their small size, simple and inexpensive synthetic routes, high aqueous solubility, their fluorescence property which make them useful for cell imaging and their high cargo loading.

In recent years, much progress has been made in terms of the synthesis, properties and applications of CNPs [17,25]. The synthesis of CNPs can be classified in two groups: chemical and physical methods. Chemical methods include electrochemical synthesis [26], acidic oxidation [4,6,27], thermal/hydrothermal synthesis [28–31] and microwave/ultrasonic synthesis [12,17,28,32]. Physical methods include arc discharge [33], laser ablation [34] and plasma treatment [35]. Chemical oxidation was commonly used to prepare fluorescent CNPs, which almost always originate from carbon-based nanomaterials. This method is easier, avoids multi-step synthesis and introduces carboxyl and hydroxyl groups on the CNP surface, making the particles negatively charged and hydrophilic. As a result, a variety of fluorescent CNPs have been prepared using food waste [36], carbon nanotubes [37], candle soot [4], carbohydrates (sucrose, glucose) [30,38], active carbon [32], orange juice, polyphenol [39,40] and honey [41]. Although numerous synthetic approaches have been developed, those that are eco-friendly and inexpensive are in demand. Furthermore, large-scale synthesis and size-controlled CNPs remain unmet technological needs.

In the field of drug delivery, carbon nanomaterials have gained considerable attention as nano-carriers due to their high surface area, enhanced cellular uptake and easy conjugation with therapeutics [42–45]. CNPs are spherical and composed of an sp^2 carbon core, which can be conjugated with chemotherapeutic drugs and biomolecules through covalent or noncovalent interactions (π–π stacking or electrostatic interactions) and used for *in vitro* and *in vivo* drug delivery applications [43,46]. However, most of the published papers to date on this topic have focused on the optical properties and *in vitro* biocompatibility of CNPs [47–50], and few have studied CNPs as delivery agents in depth [9,51,52]. Therefore, clinical application remains a challenge.

In this report, we present a green source, "black tea", as a suitable precursor for the synthesis of CNPs by nitric acid (HNO_3) oxidation. This synthesis is simple and economical because of the selection of an inexpensive carbon source. These CNPs are non-toxic; easily synthetized in large-scale production with tunable optical properties up to red spectra, which can be utilized for multiplexing applications; and can efficiently deliver doxorubicin (doxo). The biodistribution, pharmacokinetics (PK) profiles and kinetics of release suggest that CNPs-doxorubicin (Cdoxo) is an optimal drug delivery vector for cancer therapy.

2. Experimental section

2.1. Materials and instrumentation

2.1.1. Reagents

Commercially available Brooke Bond Taaza tea was utilized. HNO_3 (70%) and sodium hydroxide (NaOH) were purchased from Sigma Aldrich (St. Louis, Missouri, US), doxo was obtained from Accord Healthcare Ltd. (Durham, NC, US) and daunorubicin was purchased from Teva Pharmaceutical Industries Ltd. (Petah Tikva, Israel). All reagents were used as received without further purification. Minisart® syringe filters with a pore size of 0.2 μm were from Sartorius Stedim Biotech (Concord, CA, US), and a dialysis membrane (MWCO 0.5–1 kDa) was purchased from Spectrum Laboratories (Rancho Dominguez, CA, US) for CNP purification. LysoTracker® deep red probe was purchased from Life Technologies (Carlsbad, CA, US). Exosomes were prepared from exosome-depleted medium conditioned for 48 h and purified with an AB cell culture-nanovesicle solution according to the instructions (AB ANALITICA, Padova, Italy) [53].

DLD-1 and LoVo (colon) and MDA-MB-231 (breast) and HeLa (cervical) cancer cells were grown as indicated by the supplier (ATCC, Manassas, VA, US). Nude and FVB mice were purchased from Harlan Laboratories (Udine, Italy); the procedures were approved by the Italian Ministry of Health n°788/2015-PR and performed in accordance with the institutional guidelines. Data are reported as the mean and standard error.

2.1.2. Equipment

Water was obtained from a Milli-Q water purification system (18.2 Ω; EMD Millipore, Billerica, MA, US). UV–Vis absorption spectra were collected using a NanoDrop 2000c (Thermo Fischer Scientific, Waltham, MA, US). Fluorescence spectra were collected on an Infinite M1000 PRO and cell viability analyzed using an Infinite 200 PRO (Tecan, Männedorf, Switzerland). X-ray diffraction (XRD) data were collected on a Philips X'Pert vertical goniometer with Bragg-Brentano geometry. Transmission electron microscopy (TEM) was carried out using a Philips EM 208 microscope (Philips, Amsterdam, Netherlands). Fourier transform infrared (FT-IR) spectra were obtained on a NEXUS FT-IR spectrometer implementing a Nicolet Avatar diffuse reflectance accessory. X-ray photoelectron spectroscopy (XPS) was performed on a PHI Quantera SXM spectrometer using monochromatic Al-Kα X-ray sources at 1486.6 eV and 24.8 W with a beam diameter of 100.0 μm, a 1.2 V and 20.0 μA neutralizer, and FAT analyzer mode. Zeta potential (ζ) measurements were collected on a Zetasizer ZS90 (Malvern Instruments, Malvern, UK) using a 632 nm He-Ne laser as the light source. Fluorescence microscopy was carried out using a Nikon microscope at 20× and 40× magnification (Nikon, Chiyoda, Tokyo, Japan). The PK and biodistribution were evaluated by liquid chromatography-tandem mass spectrometry (LC-MS/MS) on a 4000 QTRAP MS/MS system equipped with a Turbo ESI source (AB Sciex, MA, USA). The exosome particle size was determined with an L10 NanoSight instrument (Malvern Instruments Ltd., UK).

2.1.3. Preparation of CNPs

CNPs were synthesized from tea in the following steps: (1) carbonization of commercial tea followed by (2) oxidation with HNO_3. The carbonized carbon was prepared by heating the commercial black tea at 200 °C for approximately 3 h, followed by evaporation of water and heating again at 200 °C for approximately 5 h. The so-formed carbonized tea powder was cooled to room temperature, dried on rotary evaporator and stored in a glass bottle. Then, 500 mg of the carbonized carbon was dispersed in HNO_3 (0.065 mol, 5 M, 13 ml) and refluxed at 80 °C for 20 h under vigorous stirring. Then, the orange solution was cooled to room temperature and centrifuged (4300*g*, 25 min, room temperature) to separate out any unreacted carbon. The orange supernatant was collected, neutralized by 5 M NaOH and filtered through a 0.2 μm Minisart® syringe. To remove salts and impurities, the raw solution was dialyzed against Milli-Q water using a dialysis membrane (MWCO 0.5–1 kDa) for at least 2 days. Finally, the obtained golden-yellow solution was dried on a rotary evaporator and used for further characterization (yield: 26%).

2.1.4. Fluorescence imaging

A droplet of an aqueous CNP dispersion (25 mg/ml) was imaged on a Nikon fluorescence microscope under different filter sets (nm), Ex 350/Em 460 (blue), Ex 490/Em 520 (green), Ex 550/Em 570 (red) and Ex 630/Em 670 (violet), at 20× magnification.

2.1.5. CNP cellular localization

The CNP cellular internalization was evaluated by plating HeLa cells at a density of 7.5×10^4 cells/slide. The next day, the cells were marked with 50 nM LysoTracker® deep red probe (Thermo Fisher, MA, US) for 2 h at 37 °C. After incubation, the cells were washed twice with 1× PBS and incubated for 24 h with 2 mg/ml CNPs. After incubation, the cells were washed twice with 1× PBS and fixed with 4% PFA for 10 min, and the slides were mounted with Alexa FluorSave solution (Thermo Fisher Scientific, Waltham MA, US). The images were obtained

on a Nikon fluorescence microscope at 40× magnification using Ex 630/Em 670 nm filters for the lysosomes and Ex 350/Em 460 nm filters for the CNPs.

2.1.6. Imaging of CNP-loaded exosomes

To load exosomes with CNPs, HeLa cells were grown until 70% confluence, treated with 2 mg/ml CNPs for 2 h, washed and then incubated in exosome-free medium for 24 h. The medium was collected, and the exosomes were extracted using an AB cell culture-nanovesicle solution. The next day, the medium was centrifuged at 103,000*g* and 4 °C for 80 min, and the pellet was resuspended in 1× PBS. The exosomes were characterized by NTA analysis (nanoparticle tracking analysis, Malvern, UK). For imaging, the exosomes loaded with CNPs were spotted on a slide and analyzed with a Nikon fluorescence microscope at 40× magnification under different filter sets (nm): Ex 350/Em 460 (blue), Ex 490/Em 520 (green), Ex 550/Em 570 (red) and Ex 630/Em 670 (violet).

2.1.7. Doxo loading efficiency and release

CNPs (0.5 mg/ml) were incubated with doxo (0.25 mg/ml) in 1× PBS for 2 h at room temperature. The unbound doxo was eliminated by centrifugation at 13000*g* for 10 min and washed twice with 1× PBS. The drug loading capacity for doxo was calculated as follows: (weight of loaded doxo)/(weight of CNPs). The weight of free doxo was measured on a UV–Vis spectrophotometer from the absorbance at 450 nm based on a doxo standard curve, and the weight of CNPs was measured from the absorbance at 289 nm based on a CNP standard curve. The release of doxo and Cdoxo (50 μg/500 μl) was evaluated using a dialysis membrane (15,000 MWCO) dipped into 1 l of 1× PBS at pH 7.4 or pH 5.5.

2.1.8. Toxicity, cytotoxicity and apoptosis tests

The toxicity of the CNPs was tested in Hela, MDA-MB-231, LoVo and DLD-1 cancer cell lines. The cytotoxicity of the free doxo, CNPs and Cdoxo was tested in MDA-MB-231, LoVo and DLD-1 cancer cell lines. Toxicity and cytotoxicity were evaluated by the CellTiter-Glo® luminescence assay (Promega, Madison, Wisconsin, US) using an Infinite 200 PRO instrument (Tecan, Switzerland). Cells were seeded in 96-well plates (Falcon BD, San Jose, CA, US) at a density of 10^3 cells/well and incubated for 24 h to allow for cell attachment. The cells were incubated with doxo, CNPs, and Cdoxo at the same drug concentrations for 96 h. The experiments were performed in triplicate. Apoptosis was evaluated after 24 h by fluorescence-activated cell sorting (FACS; BD Biosciences, San Jose, CA, US) utilizing the PE Annexin V Apoptosis Detection Kit I (BD Biosciences, San Jose, CA, US).

2.1.9. In vivo CNP toxicity and efficacy

This experiment was carried out using 8 weeks old female nude mice, which were administered by i.v. (intravenous) injection of 4 concentrations of CNPs diluted in PBS 1× (5, 10, 20 and 40 mg/kg). The body weights of the mice were monitored for >45 days.

To evaluate the anti-tumour efficacy of Cdoxo compared to doxo, 3×10^6 MDA-MB-231 cells diluted in DMEM w/o phenol red/30% matrigel HC (Corning, New York, US) were inoculated in the mammary fat pad of nude mice.

Histopathology: The organs of the mice were collected and fixed in 10% formalin buffered with PBS, embedded in paraffin, sectioned at a thickness of 3 μm and stained with hematoxylin and eosin (H&E). The tissues were analyzed with light microscopy using different magnifications.

2.1.10. PK and biodistribution

The PK experiments were performed in 8 weeks old FVB mice treated with 3 mg/kg (i.v.) of the drug diluted in PBS 1×, and approximately 100 μl of blood was collected after 0.5, 1, 3, 6, 24, 48, 96 and 192 h. Blood was collected from each mouse twice: from the mandibular vein (live mouse) and the right ventricle of the heart (sacrificed mouse). A total of 12 mice were utilized. Serum samples were stored at −80 °C. For analysis of the drug tissue distribution, the mice were sacrificed at 3 and 24 h, and their organs were washed with 10 ml of cold PBS/heparin before collection. The organs were diluted in 500 μl of 4% PBS/BSA and homogenized with a Qiagen TissueRuptor for 20 s at power 4 in ice (Qiagen, Hilden, Germany).

The doxo concentrations in serum and tissues were measured by LC-MS/MS. The proteins were precipitated with 2 volumes of cold acetonitrile containing 20 ng/ml daunorubicin as an internal standard. After vortexing and spinning at 13000 rpm for 15 min at 4 °C, the cleared supernatant was diluted with 2 volumes of 0.2% formic acid, and 10 μl of the dilution were injected into the LC-MS/MS system. Chromatographic separation was performed on an Accucore 150-C18 column (2.6 μm, 30 × 2.1 mm; Thermo Scientific, Waltham, MA USA) equilibrated with 0.2% formic acid/acetonitrile (95:5) at 0.7 ml/min and maintained at 50 °C. An elution gradient B from 5% to 80% acetonitrile was applied over 5 min. A 4000 QTRAP MS/MS system equipped with a Turbo ESI source (AB Sciex, Framingham, MA, USA) was equilibrated for 3 min in positive-ion mode. The transitions of doxo and daunorubicin were monitored in multiple reaction monitoring mode at m/z 544.1 → 397.2 and 528.2 → 321.1, respectively. The spray voltage was set at 5000 V, with a source temperature of 400 °C. The curtain gas, nebulizer gas (gas1) and auxiliary gas (gas 2) were set at 20, 50 and 50 arbitrary units, respectively. The declustering potential and collision energy voltages were set at 45 V and 16 V, respectively, for both doxo and daunorubicin.

3. Results and discussion

3.1. Characterization of CNPs prepared from black tea

The CNPs were prepared from tea by HNO_3 oxidation and characterized by UV–Vis absorption spectroscopy, fluorescence spectroscopy, powder XRD, FT-IR spectroscopy and TEM. The zeta potential of the CNPs was also measured at −16.6 mV, indicating a negative charge on the CNP surface due to the presence of carboxylic groups.

Fig. S1 shows the UV–Vis absorption and fluorescence spectra of CNPs excited at 360 nm. The UV–Vis absorption spectrum contained two distinct peaks: one at 300 nm that could be assigned to the n-π* transition of the C═O groups on the surface of the CNPs and one at 242 nm that could be assigned to π-π* transitions of the polycyclic aromatic systems (C═C) contained in the polyphenols of the tea [54]. The CNP solution produced a maximum emission peak centered at 470 nm when excited at 360 nm (Fig. S1A). To investigate the optical properties of the CNPs, emission spectra were recorded at various excitation wavelengths from 300 to 570 nm; the emission peaks were red-shifted from 390 to 570 nm while the intensities decreased (Fig. S1B, S1C). These optical properties mainly result from the different sizes and different distributions of emissive sites, which is generally a characteristic of fluorescent carbon nanomaterials [34]. The fluorescence properties of CNPs are always dependent on the size and the presence of organic functional groups in the carbon source [5].

We applied XRD and FT-IR analyses to identify the functional groups and the phase of the CNPs. The powder XRD spectrum (Fig. S2) contained a broader peak at $2\theta = 24.8°$, revealing an amorphous carbon phase in the CNPs. The FT-IR spectrum (Fig. 1A) indicated that the CNPs have many oxygen- and nitrogen-containing functional groups on their surface. The broad peak centered at 3294 cm^{-1} revealed O—H/N—H bonding, and the absorptions at 2937 and 2866 cm^{-1} could be attributed to C—H stretching vibrations. Moreover, the absorption peaks at 1652 and 1752 cm^{-1} are indicative of C═O bonds. The absorptions at 1110 and 1195 cm^{-1} could be attributed to C—O—C bonds, and the absorptions at 1318 and 1337 cm^{-1} confirm the presence of C—O bonds. Furthermore, the absorption peaks at 1594 cm^{-1} could be attributed to the C═N and C═C groups of aromatic hydrocarbons, indicating the

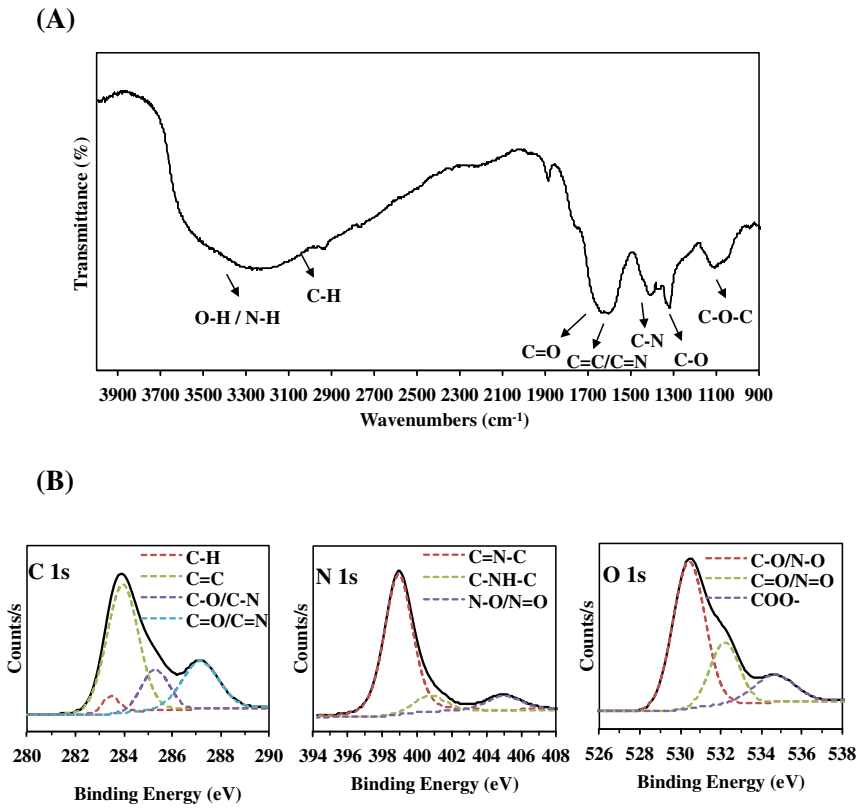

Fig. 1. (A) FT-IR spectrum of CNPs; (B) C1s, N1s, and O1s XPS spectra.

presence of sp^2 hybridization, whereas the absorption peaks at 1406 and 1431 cm^{-1} could be related to C—N bonds. These data suggest that the CNPs were functionalized with hydroxyl, alkyl, carbonyl, carboxylic, and amine groups derived from the organic molecules in the black tea and the use of HNO_3.

XPS analysis was used to confirm the functional groups on the CNP surface. From the XPS spectrum (Fig. 1B), C, N and O were detected from the peaks at 285 eV (C1s), 400.2 eV (N1 s), and 532 eV (O1s), respectively, with 62.56% carbon, 31.43% oxygen, and 6.01% nitrogen. The C1s peaks at 283.5, 284, 285.3, and 287.2 eV could be assigned to carbon in the form of C—H, sp^2 (C═ C), C—O/C—N and C═ O/C═ N, respectively [55–57]. The N1 s peaks consisted of three Gaussian peaks centered at 399, 408.8 and 405 eV, corresponding to C═ N—C, C—NH—C, and oxidized N-species such as N—O/N═ O, respectively [56,57]. The O1s peaks could be deconvoluted into three Gaussian peaks centered at 530.4, 532.2 and 534.7 eV, corresponding to C-O/N-O, C═ O/N═ O, and COO^-, respectively [57]. The surface components of the CNPs are in agreement with the FTIR results. It is well known that HNO_3 oxidation produces hydroxyl and carboxylic groups on CNP surfaces, which makes the particles water soluble and negatively charged. In addition, this oxidation can also induce nitration [58]. Our experimental data suggest that refluxing the carbonized carbon derived from tea with HNO_3 induces partial oxidation of the carbons; introduces functional groups, such as OH, COOH, and NO_2; and causes nitrogen doping into the CNPs. The introduction of functional groups imparts water solubility and a surface charge to the CNPs. This oxidation step could also be considered a chemical route to incorporating nitrogen into the CNPs, as observed from the chemical composition analysis.

The morphology and size of the CNPs were investigated by TEM. As shown in Fig. 2, the CNPs had a narrow size distribution and were spherical with an average diameter of 17 nm.

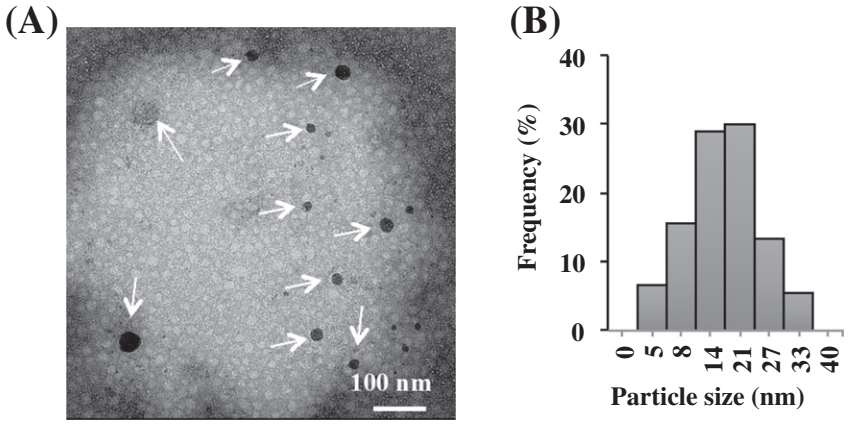

Fig. 2. (A) TEM image and (B) particle size distribution histogram of CNPs (17.3 ± 7.6 nm). Arrows indicate CNPs.

3.2. CNPs were biocompatible and suitable for bioimaging of cellular and subcellular (exosomes) compartments

The CNPs were reported to be not toxic in different experimental set-ups [26,59]. *In vitro* experiments showed that CNPs do not alter cell viability at concentrations up to 200 μg/ml [60]. A toxicity test was performed with HeLa, MDA-MB-231, LoVo and DLD-1 cells. Our CNPs were not toxic at up to 1 mg/ml, illustrating very high biocompatibility (Fig. S3), and sustained further testing in *in vivo* experiments. To strengthen these results, an apoptosis test was performed, the results of which are presented in Fig. S4. Cells were treated with 1 mg/ml CNPs, and the expression of Annexin V on the surface of the cells was measured by FACS after 24 h. No change in the percentage of apoptotic cells was observed in the CNP-treated cells over the control.

Although the CNPs were designed and synthetized for drug delivery applications. A droplet of CNPs (25 mg/ml) was deposited on a cover slip under a fluorescent microscope and imaged under different excitation wavelengths commonly utilized for biological experiments. Fluorescence of the CNPs was detected in all the ranges utilized (Fig. 3). For biological applications, a wavelength range over 600 nm is more suitable (Fig. 3D) and does not overlap with the fluorescence of doxo, which has a maximal excitation/emission of approximately 490/590 nm.

Due to the increasing number of papers focused on exosome biology and the possibility of utilizing exosomes in liquid biopsies, the CNPs were tested for use as potential fluorescent probes. Exosomes are extracellular vesicles with nanometric dimensions (30–200 nm) and diagnostic [61] and therapeutic potential [62]. Exosomes incubated with CNPs were collected after 24 h and verified by NTA analysis (Fig. S5). Equal quantities of exosomes were evaluated under fluorescence microscopy from CNP-treated and untreated cells. A clearly noticeable dotted appearance of CNP-loaded exosomes can be observed in Fig. 4 and data that is not shown here, suggesting that these CNPs can be utilized to probe exosomes for biological applications.

3.3. CNPs avoided lysosomal entrapment and delivered doxo efficiently in in vitro experiments

Lysosomal degradation is a natural process by which cells eliminate unnecessary endogenous and exogenous materials [63]. The failure of many nanomaterials is due to their accumulation inside lysosomes [64]. Escaping lysosomal degradation is a desirable functional property for drug delivery applications. Under this scope, HeLa cells were probed with LysoTracker for 2 h and incubated with 2 mg/ml CNPs for 24 h.

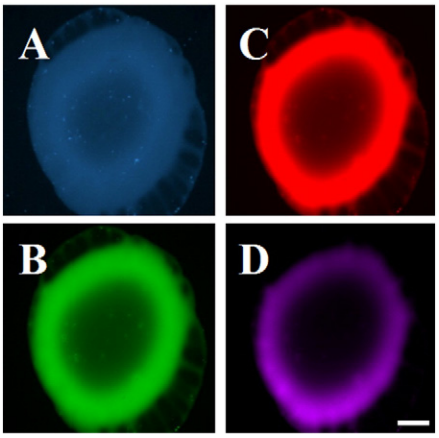

Fig. 3. (A–D) Fluorescence microscopy photographs of an aqueous solution of CNPs under different excitation filter sets: (A) 350 nm, (B) 490 nm, (C) 550 nm and (D) 630 nm. Scale bar: 200 μm.

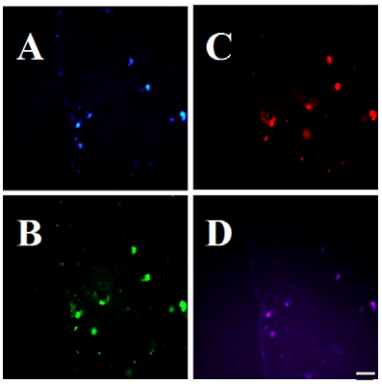

Fig. 4. Exosomes isolated from the cell culture medium of MDA-MB-231 cells treated with CNPs (2 mg/ml) for 2 h and collected after 48 h. Images were acquired with different excitation filter sets, as in Fig. 3. Scale bar: 20 μm.

Under fluorescence microscopy, the CNPs (green) had a clearly uniform distribution in the cytoplasm and nucleus, and the typically punctuated appearance of lysosomal accumulation (red) was not apparently observed (Fig. 5).

A desirable property of nanomaterials is an intrinsic ability for loading therapeutic drugs and a controlled release over time under physiological conditions [65,66]. To demonstrate this concept, the CNPs were loaded with doxo, and the kinetics of drug release was calculated from a dialysis experiment in PBS at 37 °C at different pH values. For drug loading, the CNPs were mixed with doxo at room temperature, and the drug loading was calculated to be approximately 60% (Fig. 6A). Doxo is a weak amphipathic base with pKa = 8.3. At physiological pH (7.4), the protonated fraction of doxo is still 10-fold that of the free base, while the carboxylic acid moieties on the CNP surface are nearly completely dissociated to their negative carboxylate form (pKa range: 3–5) [67,68]. Thus, the doxo molecules retain their electrostatic interactions with the CNPs at physiological pH. At pH 4, the carboxylic acid groups on the CNPs are partially dissociated, decreasing the negative charge on the CNPs and reducing the electrostatic interactions of the drug carrier with protonated doxo. To support our conclusion, CNPs were loaded with doxo at different pH levels: 4, 5.5 and 7.4 (Fig. S6). The percentage of loading positively correlated with the pH.

The extracellular pH (pHe) of tumour tissues is acidified by the metabolism of tumour cells [69]. Cell survival is conditioned by maintenance of a favourable acid-base balance (pH). Because of cellular metabolism, which produces CO_2 and lactic acid, cancer cells are continuously exposed to large acid-base fluxes, which would disturb the pH. In contrast to normal cells, most tumour cells preferentially convert glucose and other substrates to lactic acid, even under aerobic conditions.

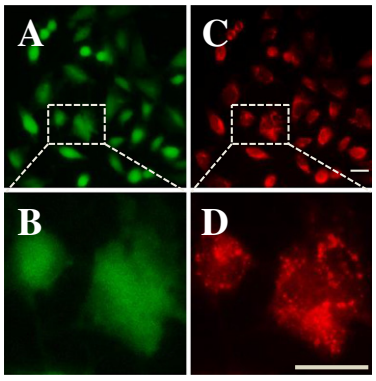

Fig. 5. HeLa cells (A) treated with 2 mg/ml CNPs after 24 h and marked with (C) LysoTracker. (B) and (D) Zoom-in of (A) and (C). Scale bar: 20 μm.

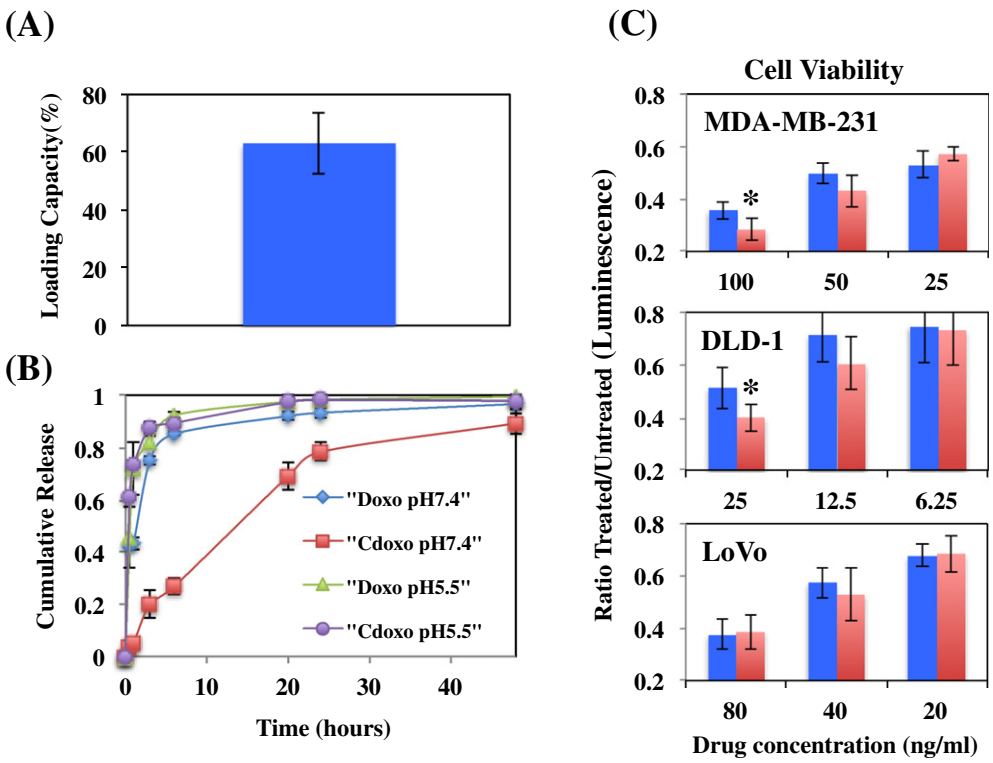

Fig. 6. (A) Loading capacity of Cdoxo. The graph displays the percentage of doxo loading (y-axis) (B) Release of doxo from CNPs. The cumulative release of doxo was evaluated by measuring the fluorescence of doxo, which resides inside the dialysis membrane at each time point at pH 5.5 and 7.4. (C) Cytotoxic effects of Cdoxo on MDA-MB-231, DLD-1 and LoVo cell lines treated with increasing concentrations of doxo (blue) or Cdoxo (red), as indicated on the x-axis (ng/ml). *p value <0.05 (y-axis). The quantity of utilized doxo was based on previously calculated IC50 (middle value).

This phenomenon, termed "the Warburg effect", was reported by Warburg and co-workers in the 1920s [70–72]. Due to increased glucose metabolism, tumours possess a greater capacity to pump lactic acid and protons out to the extracellular spaces to maintain an appropriate neutral-alkaline intracellular pH (pHi), which is essential for cell vitality. The inefficient removal of protons and lactic acid from extracellular spaces creates a reversed gradient characterized by an acidic pHe and alkaline pHi [73–75]. *In vitro* and *in vivo* studies revealed that tumour cells have a pHi ranging from 7.1 to 7.6 (pHi of normal cells: 7.0 to 7.2) and a pHe of 6.2–6.9 (pHe of normal extracellular space: 7.3–7.4) [76]. The intravesicular pH along the endocytic pathway ranges from pH 6.0–6.5 in early endosomes to pH 4.5–5.5 in late endosomes and lysosomes [77].

A drug delivery system that is able to release its cargo more efficiently around the tumour site at low pH (approximately pH 6) represents an intelligent system to specifically target tumour cells [78]. To study the capacity and release of Cdoxo over different pH gradients, we carried out a release experiment at pH 5.5 and 7.4 to mimic the bloodstream, tumour microenvironments and intracellular endosome/lysosome pathway (Fig. 6B) [79,80]. The release of doxo was derived from a log-log plot of the cumulative release *versus* time. Noticeably, the CNPs maintained a stable interaction with doxo at alkaline pH (pH of the bloodstream) with a slow release profile (approximately 15 h), compared to a fast release profile (approximately 1 h) when the medium was acidified to levels of the extracellular space of the tumour and in subcellular compartments. This pH gradient increases the ratio of the tumoral/non-tumoral drug concentration, thereby elevating the therapeutic index of doxo.

Subsequently, the cell viability of MDA-MB-231, LoVo and DLD-1 cells treated with Cdoxo was tested. Cells were treated with 3 different concentrations of free doxo or Cdoxo, and the cell viability was assessed after 96 h (Fig. 6C). Cdoxo exhibited better cytotoxicity than free doxo in MDA-MB-231 and DLD-1 cells (p value < 0.05). Based on these results, we further evaluated the CNPs as a drug delivery system in a mouse model of breast cancer.

3.4. CNPs were not toxic in mice and increased the efficacy of doxo

In vitro experiments demonstrated that our CNPs were not toxic at concentrations above the necessary dosage for drug delivery applications. To better predict toxicity in humans, nude mice were treated with a single i.v. injection of 5, 10, 20 and 40 mg/kg CNPs. Their body weight was monitored as an objective parameter of mice wellness. The mice were followed over a period of approximately 2 months. We did not observe any symptoms of stress or clinical illness. The body weight of the mice increased during the observational period (Fig. 7A). After >6 months, the mice were sacrificed, and their tissues were histopathologically analyzed. No obvious signs of toxicity were observed (Fig. S7).

Supported by this encouraging data, MDA-MB-231 cells were orthotopically inoculated in the mammary fat pad of nude mice. After the tumours had reached an average volume of 57 ± 8 mm^3, the mice were treated 3 times on a weekly base with 3 mg/kg Cdoxo or free doxo. Fig. 7B demonstrates that the tumour volume of the Cdoxo-treated mice was reduced compared to the tumours of mice treated with free doxo (p value < 0.05). The body weight of the mice was similar among the groups of mice tested during the experiment (Fig. 7C).

3.5. CNPs altered the biodistribution and prolonged the circulation time of doxo

Data obtained from well-known and successful liposomal formulations revealed that drug efficacy can be increased by a longer circulation time, avoiding rapid clearance [81]. To investigate the potential changes in the PK profile, we administered 3 mg/kg doxo (i.v.) and Cdoxo to FVB/

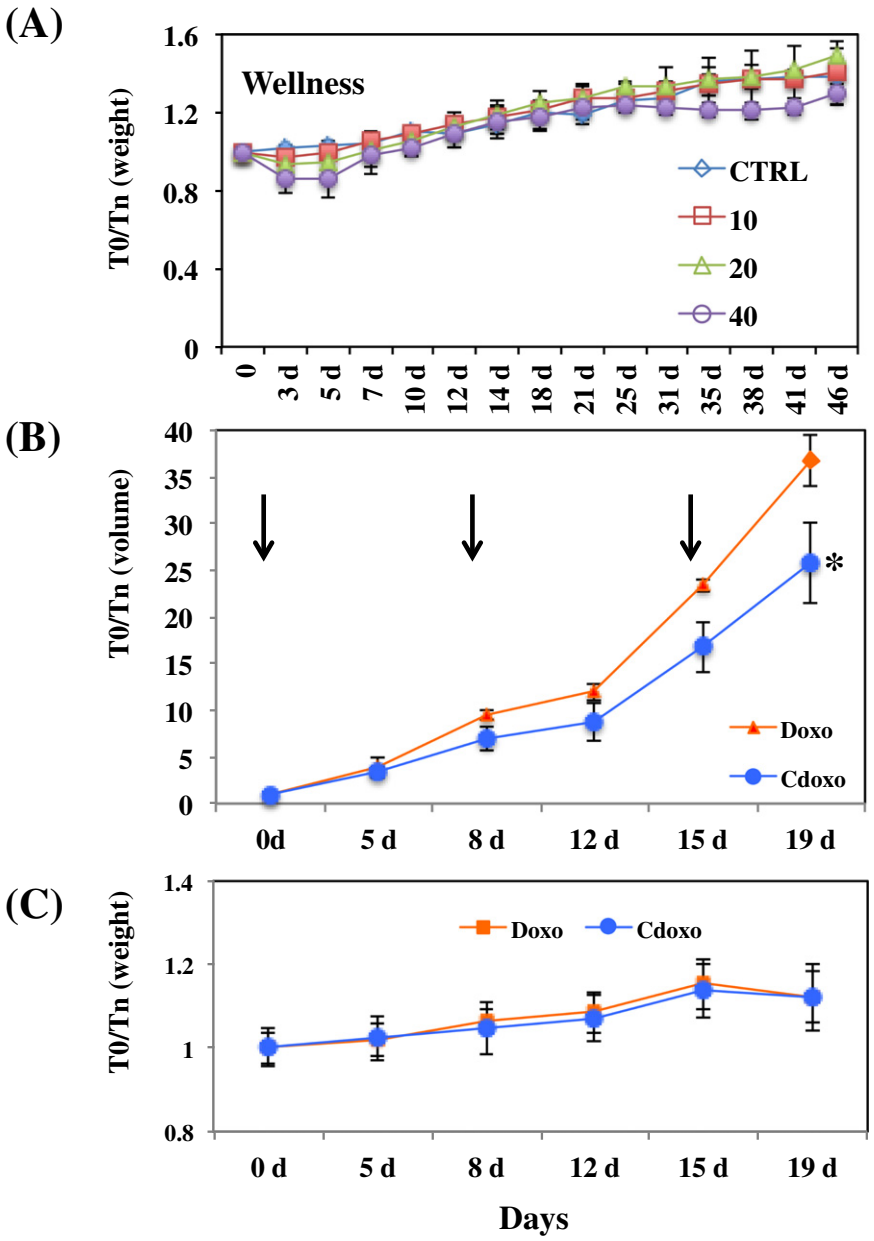

Fig. 7. (A) Weight of mice treated with different concentrations (mg/kg) of CNPs as indicated. (B) Mice were treated 3 times (arrows) at 3 mg/kg Cdoxo or free doxo, and the tumour volume was measured (y-axis). *p value < 0.05 (C) Weight of mice treated as in (B). T_0: time at the beginning of the experiment; T_n: time on day n as indicated. Eight tumours were analyzed per data point.

N mice. The PK profile of doxo in blood and tissues was qualitatively similar when administered as the free drug or Cdoxo. Both PK profiles were characterized by fast first-phase elimination. However, in the late phase of elimination, up to 4 days, the concentration of doxo in blood remained higher when administered as Cdoxo (Fig. 8A) compared to free doxo. This result is consistent with the increase in the mean residence time from 14.1 ± 2 to 20.1 ± 0.5 h (p value < 0.01) and the apparent constant elimination from 0.07 ± 0.01 h^{-1} to 0.050 ± 0.01 h^{-1} (p value < 0.05) for free doxo and Cdoxo, respectively.

The tissue distribution of the drug 3 h post-injection demonstrated a similar profile between Cdoxo and free doxo, except in the skin (Fig. 8B). After 24 h, the distribution of Cdoxo changed, with an accumulation in the liver and intestine and a reduction in the skin (p value < 0.05; Fig. 8C). These data suggest that Cdoxo could reduce the skin toxicity associated with liposomal formulations of doxo and be utilized to treat gastro-intestinal cancers.

4. Conclusions

In this study, we prepared a new nanovector that can be used to image subcellular compartments such as exosomes with excellent properties for drug delivery [82]. These CNPs can be efficiently loaded with doxo, a widely used chemotherapeutic drug, and exhibit controlled release under acidic conditions, as in the tumour microenvironment. Cdoxo was more effective *in vivo* than free doxo due to a different PK profile. Hence, a simple and green synthesis starting from tea could produce a tunable and safe drug delivery nanocarrier with excellent biocompatible properties.

Funding sources

My First AIRC (No. 1569)

AIRC Special Program Molecular Clinical Oncology, 5 × 1000, (No. 12214)

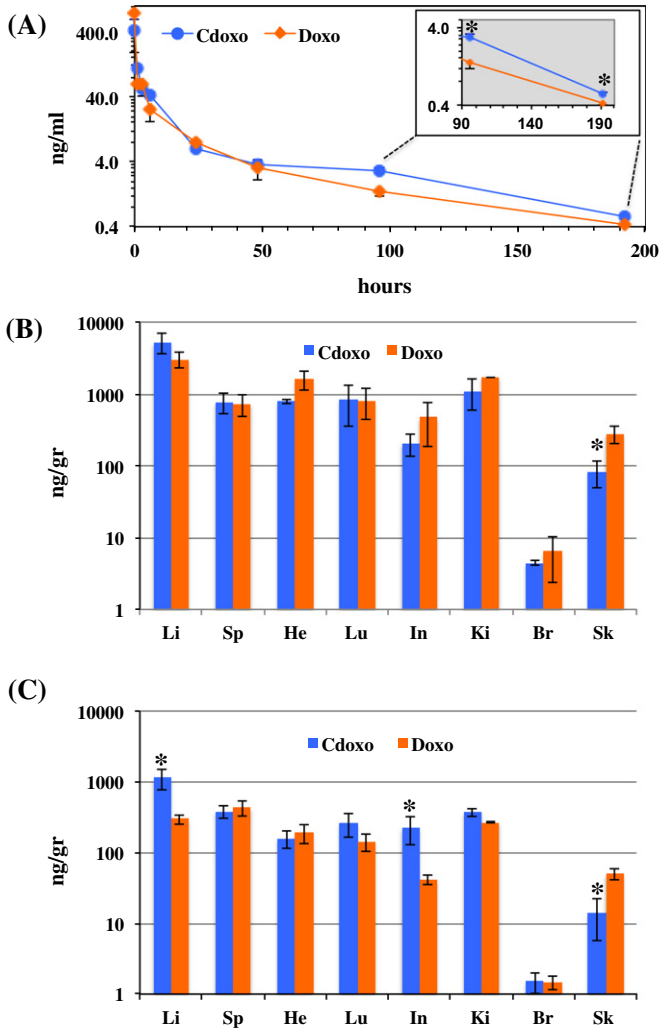

Fig. 8. (A) PK profile of free doxo and Cdoxo at 0.5, 1, 3, 6, 24, 48, 96 and 192 h. In the insert, the time points 96 and 192 h were zoomed in. *p value < 0.05. (B) and (C) Biodistribution of free doxo and Cdoxo at 3 (B) and 24 (C) hours. At 3 h, less Cdoxo was present in the skin. At 24 h, increased accumulation of Cdoxo in the liver and intestine was observed. The y-axis is in logarithmic scale (ng/g of drug/tissue). Li: liver, Sp: spleen, He: heart, Lu: lung, In: intestine, Ki: kidney, Br: brain, Sk: skin. Three mice were utilized for each data point.

Italian Ministry of Education MIUR (FIRB prot. RBAP11ETKA)

Competing interests

The authors declare no competing interests.

Acknowledgements

The authors are thankful to My First AIRC (No. 1569); AIRC Special Program Molecular Clinical Oncology, 5 × 1000, (No. 12214); and Italian Ministry of Education MIUR (FIRB prot. RBAP11ETKA) for funding.

References

[1] T. Muthukumar, S. Prabhavathi, M. Chamundeeswari, T.P. Sastry, Bio-modified carbon nanoparticles loaded with methotrexate possible carrier for anticancer drug delivery, Mater. Sci. Eng. C Mater. Biol. Appl. 36 (2014) 14–19, http://dx.doi.org/10.1016/j.msec.2013.11.046.

[2] G. Sponchia, E. Ambrosi, F. Rizzolio, M. Hadla, A. Del Tedesco, C.R. Spena, et al., Biocompatible tailored zirconia mesoporous nanoparticles with high surface area for theranostic applications, J. Mater. Chem. B 3 (2015) 7300–7306, http://dx.doi.org/10.1039/C5TB01424G.

[3] Y. Zhu, J. Li, W. Li, Y. Zhang, X. Yang, N. Chen, et al., The biocompatibility of nanodiamonds and their application in drug delivery systems, Theranostics 2 (2012) 302–312, http://dx.doi.org/10.7150/thno.3627.

[4] H. Liu, T. Ye, C. Mao, Fluorescent carbon nanoparticles derived from candle soot, Angew. Chem. Int. Ed. Eng. 46 (2007) 6473–6475, http://dx.doi.org/10.1002/anie.200701271.

[5] V. Kumar, G. Toffoli, F. Rizzolio, Fluorescent carbon nanoparticles in medicine for cancer therapy, ACS Med. Chem. Lett. 4 (2013) 1012–1013, http://dx.doi.org/10.1021/ml400394a.

[6] S.K. Bhunia, A. Saha, A.R. Maity, S.C. Ray, N.R. Jana, Carbon nanoparticle-based fluorescent bioimaging probes, Sci. Rep. 3 (2013) 1473, http://dx.doi.org/10.1038/srep01473.

[7] L. Cao, S.-T. Yang, X. Wang, P.G. Luo, J.-H. Liu, S. Sahu, et al., Competitive performance of carbon "quantum" dots in optical bioimaging, Theranostics 2 (2012) 295–301, http://dx.doi.org/10.7150/thno.3912.

[8] S.E. Skrabalak, Ultrasound-assisted synthesis of carbon materials, Phys. Chem. Chem. Phys. 11 (2009) 4930–4942, http://dx.doi.org/10.1039/b823408f.

[9] H.U. Lee, S.Y. Park, E.S. Park, B. Son, S.C. Lee, J.W. Lee, et al., Photoluminescent carbon nanotags from harmful cyanobacteria for drug delivery and imaging in cancer cells, Sci. Rep. 4 (2014) 4665, http://dx.doi.org/10.1038/srep04665.

[10] Q. Zeng, D. Shao, X. He, Z. Ren, W. Ji, C. Shan, et al., Carbon dots as a trackable drug delivery carrier for localized cancer therapy in vivo, J. Mater. Chem. B 4 (2016) 5119–5126, http://dx.doi.org/10.1039/C6TB01259K.

[11] Z. Zhang, Y. Shi, Y. Pan, X. Cheng, L. Zhang, J. Chen, et al., Quinoline derivative-functionalized carbon dots as a fluorescent nanosensor for sensing and intracellular imaging of Zn^{2+}, J. Mater. Chem. B 2 (2014) 5020, http://dx.doi.org/10.1039/C4TB00677A.

[12] L. Zhou, Y. Lin, Z. Huang, J. Ren, X. Qu, Carbon nanodots as fluorescence probes for rapid, sensitive, and label-free detection of Hg^{2+} and biothiols in complex matrices, Chem. Commun. (Camb.) 48 (2012) 1147–1149, http://dx.doi.org/10.1039/c2cc16791c.

[13] Q. Qu, A. Zhu, X. Shao, G. Shi, Y. Tian, Development of a carbon quantum dots-based fluorescent Cu^{2+} probe suitable for living cell imaging, Chem. Commun. (Camb.) 48 (2012) 5473–5475, http://dx.doi.org/10.1039/c2cc31000g.

[14] Y. Jiao, B. Zhu, J. Chen, X. Duan, Fluorescent sensing of fluoride in cellular system, Theranostics 5 (2015) 173–187, http://dx.doi.org/10.7150/thno.9860.

[15] L. Tang, R. Ji, X. Cao, J. Lin, H. Jiang, X. Li, et al., Deep ultraviolet photoluminescence of water-soluble self-passivated graphene quantum dots, ACS Nano 6 (2012) 5102–5110, http://dx.doi.org/10.1021/nn300760g.

[16] L. Cao, S. Sahu, P. Anilkumar, C.E. Bunker, J. Xu, K.A.S. Fernando, et al., Carbon nanoparticles as visible-light photocatalysts for efficient CO_2 conversion and beyond, J. Am. Chem. Soc. 133 (2011) 4754–4757, http://dx.doi.org/10.1021/ja200804h.

[17] S.N. Baker, G.A. Baker, Luminescent carbon nanodots: emergent nanolights, Angew. Chem. Int. Ed. Eng. 49 (2010) 6726–6744, http://dx.doi.org/10.1002/anie.200906623.

[18] X. Michalet, F.F. Pinaud, L.A. Bentolila, J.M. Tsay, S. Doose, J.J. Li, et al., Quantum dots for live cells, in vivo imaging, and diagnostics, Science 307 (2005) 538–544, http://dx.doi.org/10.1126/science.1104274.

[19] R. Hardman, A toxicologic review of quantum dots: toxicity depends on physicochemical and environmental factors, Environ. Health Perspect. 114 (2006) 165–172.

[20] S. Vardharajula, S.Z. Ali, P.M. Tiwari, E. Eroğlu, K. Vig, V.A. Dennis, et al., Functionalized carbon nanotubes: biomedical applications, Int. J. Nanomedicine 7 (2012) 5361–5374, http://dx.doi.org/10.2147/IJN.S35832.

[21] X. Zhang, L. Meng, Q. Lu, Z. Fei, P.J. Dyson, Targeted delivery and controlled release of doxorubicin to cancer cells using modified single wall carbon nanotubes, Biomaterials 30 (2009) 6041–6047, http://dx.doi.org/10.1016/j.biomaterials.2009.07.025.

[22] Z. Liu, A.C. Fan, K. Rakhra, S. Sherlock, A. Goodwin, X. Chen, et al., Supramolecular stacking of doxorubicin on carbon nanotubes for in vivo cancer therapy, Angew. Chem. Int. Ed. 48 (2009) 7668–7672, http://dx.doi.org/10.1002/anie.200902612.

[23] M.J. Mitchell, C.A. Castellanos, M.R. King, M.J. Mitchell, C.A. Castellanos, M.R. King, Nanostructured surfaces to target and kill circulating tumor cells while repelling leukocytes, J. Nanomater. 2012 (2012)http://dx.doi.org/10.1155/2012/831263.

[24] M.J. Mitchell, C.S. Chen, V. Ponmudi, A.D. Hughes, M.R. King, E-selectin liposomal and nanotube-targeted delivery of doxorubicin to circulating tumor cells, J. Control. Release 160 (2012) 609–617, http://dx.doi.org/10.1016/j.jconrel.2012.02.018.

[25] J. Shen, Y. Zhu, X. Yang, C. Li, Graphene quantum dots: emergent nanolights for bioimaging, sensors, catalysis and photovoltaic devices, Chem. Commun. (Camb.) 48 (2012) 3686–3699, http://dx.doi.org/10.1039/c2cc00110a.

[26] Q.-L. Zhao, Z.-L. Zhang, B.-H. Huang, J. Peng, M. Zhang, D.-W. Pang, Facile preparation of low cytotoxicity fluorescent carbon nanocrystals by electrooxidation of graphite, Chem. Commun. (Camb.) (2008) 5116–5118, http://dx.doi.org/10.1039/b812420e.

[27] X. Tu, Y. Ma, Y. Cao, J. Huang, M. Zhang, Z. Zhang, PEGylated carbon nanoparticles for efficient in vitro photothermal cancer therapy, J. Mater. Chem. B 2 (2014) 2184, http://dx.doi.org/10.1039/c3tb21750g.

[28] R. Liu, H. Li, W. Kong, J. Liu, Y. Liu, C. Tong, et al., Ultra-sensitive and selective Hg^{2+} detection based on fluorescent carbon dots, Mater. Res. Bull. 48 (2013) 2529–2534, http://dx.doi.org/10.1016/j.materresbull.2013.03.015.

[29] Y. Guo, L. Zhang, S. Zhang, Y. Yang, X. Chen, M. Zhang, Fluorescent carbon nanoparticles for the fluorescent detection of metal ions, Biosens. Bioelectron. 63 (2015) 61–71, http://dx.doi.org/10.1016/j.bios.2014.07.018.

[30] H.K. Sadhanala, J. Khatei, K.K. Nanda, Facile hydrothermal synthesis of carbon nanoparticles and possible application as white light phosphors and catalysts for the reduction of nitrophenol, RSC Adv. 4 (2014) 11481, http://dx.doi.org/10.1039/c3ra47527a.
[31] X. He, H. Li, Y. Liu, H. Huang, Z. Kang, S.-T. Lee, Water soluble carbon nanoparticles: hydrothermal synthesis and excellent photoluminescence properties, Colloids Surf. B: Biointerfaces 87 (2011) 326–332, http://dx.doi.org/10.1016/j.colsurfb.2011.05.036.
[32] H. Li, X. He, Y. Liu, H. Yu, Z. Kang, S.-T. Lee, Synthesis of fluorescent carbon nanoparticles directly from active carbon via a one-step ultrasonic treatment, Mater. Res. Bull. 46 (2011) 147–151, http://dx.doi.org/10.1016/j.materresbull.2010.10.013.
[33] X. Xu, R. Ray, Y. Gu, H.J. Ploehn, L. Gearheart, K. Raker, et al., Electrophoretic analysis and purification of fluorescent single-walled carbon nanotube fragments, J. Am. Chem. Soc. 126 (2004) 12736–12737, http://dx.doi.org/10.1021/ja040082h.
[34] Y.-P. Sun, B. Zhou, Y. Lin, W. Wang, K.A.S. Fernando, P. Pathak, et al., Quantum-sized carbon dots for bright and colorful photoluminescence, J. Am. Chem. Soc. 128 (2006) 7756–7757, http://dx.doi.org/10.1021/ja062677d.
[35] H. Jiang, F. Chen, M.G. Lagally, F.S. Denes, New strategy for synthesis and functionalization of carbon nanoparticles, Langmuir 26 (2010) 1991–1995, http://dx.doi.org/10.1021/la9022163.
[36] S.Y. Park, H.U. Lee, E.S. Park, S.C. Lee, J.-W. Lee, S.W. Jeong, et al., Photoluminescent green carbon nanodots from food-waste-derived sources: large-scale synthesis, properties, and biomedical applications, ACS Appl. Mater. Interfaces 6 (2014) 3365–3370, http://dx.doi.org/10.1021/am500159p.
[37] M.H. Rümmeli, A. Bachmatiuk, F. Börrnert, F. Schäffel, I. Ibrahim, K. Cendrowski, et al., Synthesis of carbon nanotubes with and without catalyst particles, Nanoscale Res. Lett. 6 (2011) 303, http://dx.doi.org/10.1186/1556-276X-6-303.
[38] H. Li, X. He, Y. Liu, H. Huang, S. Lian, S.-T. Lee, et al., One-step ultrasonic synthesis of water-soluble carbon nanoparticles with excellent photoluminescent properties, Carbon 49 (2011) 605–609, http://dx.doi.org/10.1016/j.carbon.2010.10.004.
[39] S. Sahu, B. Behera, T.K. Maiti, S. Mohapatra, Simple one-step synthesis of highly luminescent carbon dots from orange juice: application as excellent bio-imaging agents, Chem. Commun. (Camb.) 48 (2012) 8835–8837, http://dx.doi.org/10.1039/c2cc33796g.
[40] A. Konwar, N. Gogoi, G. Majumdar, D. Chowdhury, Green chitosan-carbon dots nanocomposite hydrogel film with superior properties, Carbohydr. Polym. 115 (2015) 238–245, http://dx.doi.org/10.1016/j.carbpol.2014.08.021.
[41] L. Wu, M. Luderer, X. Yang, C. Swain, H. Zhang, K. Nelson, et al., Surface passivation of carbon nanoparticles with branched macromolecules influences near infrared bioimaging, Theranostics 3 (2013) 677–686, http://dx.doi.org/10.7150/thno.6535.
[42] J. Shi, H. Zhang, L. Wang, L. Li, H. Wang, Z. Wang, et al., PEI-derivatized fullerene drug delivery using folate as a homing device targeting to tumor, Biomaterials 34 (2013) 251–261, http://dx.doi.org/10.1016/j.biomaterials.2012.09.039.
[43] F. Karchemski, D. Zucker, Y. Barenholz, O. Regev, Carbon nanotubes-liposomes conjugate as a platform for drug delivery into cells, J. Control. Release 160 (2012) 339–345, http://dx.doi.org/10.1016/j.jconrel.2011.12.037.
[44] B.S. Wong, S.L. Yoong, A. Jagusiak, T. Panczyk, H.K. Ho, W.H. Ang, et al., Carbon nanotubes for delivery of small molecule drugs, Adv. Drug Deliv. Rev. 65 (2013) 1964–2015, http://dx.doi.org/10.1016/j.addr.2013.08.005.
[45] J. Shi, L. Wang, J. Gao, Y. Liu, J. Zhang, R. Ma, et al., A fullerene-based multi-functional nanoplatform for cancer theranostic applications, Biomaterials 35 (2014) 5771–5784, http://dx.doi.org/10.1016/j.biomaterials.2014.03.071.
[46] M. Ajmal, U. Yunus, A. Matin, N.U. Haq, Synthesis, characterization and in vitro evaluation of methotrexate conjugated fluorescent carbon nanoparticles as drug delivery system for human lung cancer targeting, J. Photochem. Photobiol. B 153 (2015) 111–120, http://dx.doi.org/10.1016/j.jphotobiol.2015.09.006.
[47] S.-T. Yang, L. Cao, P.G. Luo, F. Lu, X. Wang, H. Wang, et al., Carbon dots for optical imaging in vivo, J. Am. Chem. Soc. 131 (2009) 11308–11309, http://dx.doi.org/10.1021/ja904843x.
[48] S. Zhu, Q. Meng, L. Wang, J. Zhang, Y. Song, H. Jin, et al., Highly photoluminescent carbon dots for multicolor patterning, sensors, and bioimaging, Angew. Chem. Int. Ed. Eng. 52 (2013) 3953–3957, http://dx.doi.org/10.1002/anie.201300519.
[49] J. Wang, P. Zhang, C. Huang, G. Liu, K.C.-F. Leung, Y.X.J. Wáng, High performance photoluminescent carbon dots for in vitro and in vivo bioimaging: effect of nitrogen doping ratios, Langmuir 31 (2015) 8063–8073, http://dx.doi.org/10.1021/acs.langmuir.5b01875.
[50] X. Huang, F. Zhang, L. Zhu, K.Y. Choi, N. Guo, J. Guo, et al., Effect of injection routes on the biodistribution, clearance, and tumor uptake of carbon dots, ACS Nano 7 (2013) 5684–5693, http://dx.doi.org/10.1021/nn401911k.
[51] A. Mewada, S. Pandey, M. Thakur, D. Jadhav, M. Sharon, Swarming carbon dots for folic acid mediated delivery of doxorubicin and biological imaging, J. Mater. Chem. B 2 (2014) 698–705, http://dx.doi.org/10.1039/C3TB21436B.
[52] M. Zheng, S. Liu, J. Li, D. Qu, H. Zhao, X. Guan, et al., Integrating oxaliplatin with highly luminescent carbon dots: an unprecedented theranostic agent for personalized medicine, Adv. Mater. 26 (2014) 3554–3560, http://dx.doi.org/10.1002/adma.201306192.
[53] M. Hadla, S. Palazzolo, G. Corona, I. Caligiuri, V. Canzonieri, G. Toffoli, et al., Exosomes increase the therapeutic index of doxorubicin in breast and ovarian cancer mouse models, Nanomedicine (London) 11 (2016) 2431–2441, http://dx.doi.org/10.2217/nnm-2016-0154.
[54] X. Wen, P. Yu, Y.-R. Toh, X. Hao, J. Tang, Intrinsic and extrinsic fluorescence in carbon nanodots: ultrafast time-resolved fluorescence and carrier dynamics, Adv. Opt. Mater. 1 (2013) 173–178, http://dx.doi.org/10.1002/adom.201200046.
[55] S. Liu, J. Tian, L. Wang, Y. Luo, J. Zhai, X. Sun, et al., Preparation of photoluminescent carbon nitride dots from CCl4 and 1,2-ethylenediamine: a heat-treatment-based strategy, J. Mater. Chem. 21 (2011) 11726, http://dx.doi.org/10.1039/c1jm12149a.
[56] M. Tan, X. Li, H. Wu, B. Wang, J. Wu, N-doped carbon dots derived from bovine serum albumin and formic acid with one- and two-photon fluorescence for live cell nuclear imaging, Colloids Surf. B: Biointerfaces 136 (2015) 141–149, http://dx.doi.org/10.1016/j.colsurfb.2015.09.008.
[57] S.C. Ray, A. Saha, N.R. Jana, R. Sarkar, Fluorescent carbon nanoparticles: synthesis, characterization, and bioimaging application, J. Phys. Chem. C 113 (2009) 18546–18551, http://dx.doi.org/10.1021/jp905912n.
[58] I.I. Salame, T.J. Bandosz, Surface chemistry of activated carbons: combining the results of temperature-programmed desorption, Boehm, and potentiometric titrations, J. Colloid Interface Sci. 240 (2001) 252–258, http://dx.doi.org/10.1006/jcis.2001.7596.
[59] S.-T. Yang, X. Wang, H. Wang, F. Lu, P.G. Luo, L. Cao, et al., Carbon dots as nontoxic and high-performance fluorescence imaging agents, J. Phys. Chem. C Nanomater. Interfaces 113 (2009) 18110–18114, http://dx.doi.org/10.1021/jp9085969.
[60] J. Ge, Q. Jia, W. Liu, L. Guo, Q. Liu, M. Lan, et al., Red-emissive carbon dots for fluorescent, photoacoustic, and thermal theranostics in living mice, Adv. Mater. 27 (2015) 4169–4177, http://dx.doi.org/10.1002/adma.201500323.
[61] S.A. Melo, L.B. Luecke, C. Kahlert, A.F. Fernandez, S.T. Gammon, J. Kaye, et al., Glypican-1 identifies cancer exosomes and detects early pancreatic cancer, Nature 523 (2015) 177–182, http://dx.doi.org/10.1038/nature14581.
[62] G. Toffoli, M. Hadla, G. Corona, I. Caligiuri, S. Palazzolo, S. Semeraro, et al., Exosomal doxorubicin reduces the cardiac toxicity of doxorubicin, Nanomedicine (London) 10 (2015) 2963–2971, http://dx.doi.org/10.2217/nnm.15.118.
[63] E.-L. Eskelinen, P. Saftig, Autophagy: a lysosomal degradation pathway with a central role in health and disease, Biochim. Biophys. Acta, Mol. Cell Res. 1793 (2009) 664–673, http://dx.doi.org/10.1016/j.bbamcr.2008.07.014.
[64] D. Huang, H. Zhou, J. Gao, Nanoparticles modulate autophagic effect in a dispersity-dependent manner, Sci. Rep. 5 (2015) 14361, http://dx.doi.org/10.1038/srep14361.
[65] J. Wolfram, H. Shen, M. Ferrari, Multistage vector (MSV) therapeutics, J. Control. Release 219 (2015) 406–415, http://dx.doi.org/10.1016/j.jconrel.2015.08.010.
[66] E. Blanco, H. Shen, M. Ferrari, Principles of nanoparticle design for overcoming biological barriers to drug delivery, Nat. Biotechnol. 33 (2015) 941–951, http://dx.doi.org/10.1038/nbt.3330.
[67] B.G. Tehan, E.J. Lloyd, M.G. Wong, W.R. Pitt, J.G. Montana, D.T. Manallack, et al., Estimation of pKa using semiempirical molecular orbital methods. Part 1: application to phenols and carboxylic acids, Quant. Struct. Relationships 21 (2002) 457–472, http://dx.doi.org/10.1002/1521-3838(200211)21:5<457::AID-QSAR457>3.0.CO;2-5.
[68] J. Reijenga, A. van Hoof, A. van Loon, B. Teunissen, Development of methods for the determination of pKa values, Anal. Chem. Insights 8 (2013) 53–71, http://dx.doi.org/10.4137/ACI.S12304.
[69] Y. Kato, S. Ozawa, C. Miyamoto, Y. Maehata, A. Suzuki, T. Maeda, et al., Acidic extracellular microenvironment and cancer, Cancer Cell Int. 13 (2013) 89, http://dx.doi.org/10.1186/1475-2867-13-89.
[70] M.G. Vander Heiden, L.C. Cantley, C.B. Thompson, Understanding the Warburg effect: the metabolic requirements of cell proliferation, Science 324 (2009) 1029–1033, http://dx.doi.org/10.1126/science.1160809.
[71] R.A. Gatenby, R.J. Gillies, Why do cancers have high aerobic glycolysis? Nat. Rev. Cancer 4 (2004) 891–899, http://dx.doi.org/10.1038/nrc1478.
[72] O. Warburg, F. Wind, E. Negelein, The metabolism of tumors in the body, J. Gen. Physiol. 8 (1927) 519–530.
[73] L.E. Gerweck, K. Seetharaman, Cellular pH gradient in tumor versus normal tissue: potential exploitation for the treatment of cancer, Cancer Res. 56 (1996) 1194–1198.
[74] A. Hulikova, A.L. Harris, R.D. Vaughan-Jones, P. Swietach, Regulation of intracellular pH in cancer cell lines under normoxia and hypoxia, J. Cell. Physiol. 228 (2013) 743–752, http://dx.doi.org/10.1002/jcp.24221.
[75] A.I. Hashim, X. Zhang, J.W. Wojtkowiak, G.V. Martinez, R.J. Gillies, Imaging pH and metastasis, NMR Biomed. 24 (2011) 582–591, http://dx.doi.org/10.1002/nbm.1644.
[76] M.V. Shirmanova, I.N. Druzhkova, M.M. Lukina, M.E. Matlashov, V.V. Belousov, L.B. Snopova, et al., Intracellular pH imaging in cancer cells in vitro and tumors in vivo using the new genetically encoded sensor SypHer2, Biochim. Biophys. Acta 1850 (2015) 1905–1911, http://dx.doi.org/10.1016/j.bbagen.2015.05.001.
[77] A. Sorkin, M. Von Zastrow, Signal transduction and endocytosis: close encounters of many kinds, Nat. Rev. Mol. Cell Biol. 3 (2002) 600–614, http://dx.doi.org/10.1038/nrm883.
[78] Z. Wang, J. Xia, C. Zhou, B. Via, Y. Xia, F. Zhang, et al., Synthesis of strongly green-photoluminescent graphene quantum dots for drug carrier, Colloids Surf. B: Biointerfaces 112 (2013) 192–196, http://dx.doi.org/10.1016/j.colsurfb.2013.07.025.
[79] A.R. Chowdhuri, T. Singh, S.K. Ghosh, S.K. Sahu, Carbon dots embedded magnetic nanoparticles @chitosan @metal organic framework as a nanoprobe for pH sensitive targeted anticancer drug delivery, ACS Appl. Mater. Interfaces 8 (2016) 16573–16583, http://dx.doi.org/10.1021/acsami.6b03988.
[80] Z. Liu, X. Sun, N. Nakayama-Ratchford, H. Dai, Supramolecular chemistry on water-soluble carbon nanotubes for drug loading and delivery, ACS Nano 1 (2007) 50–56, http://dx.doi.org/10.1021/nn700040t.
[81] A.T. Horowitz, Y. Barenholz, A.A. Gabizon, In vitro cytotoxicity of liposome-encapsulated doxorubicin: dependence on liposome composition and drug release, Biochim. Biophys. Acta 1109 (1992) 203–209, http://dx.doi.org/10.1016/0005-2736(92)90084-Y.
[82] S. Kunjachan, J. Ehling, G. Storm, F. Kiessling, T. Lammers, Noninvasive imaging of nanomedicines and nanotheranostics: principles, progress, and prospects, Chem. Rev. 115 (2015) 10907–10937, http://dx.doi.org/10.1021/cr500314d.